

ACCEPTED MANUSCRIPT

High-density electrophysiological recordings in macaque using a chronically implanted 128-channel passive silicon probe

To cite this article before publication: Liane Klein *et al* 2020 *J. Neural Eng.* in press <https://doi.org/10.1088/1741-2552/ab8436>

Manuscript version: Accepted Manuscript

Accepted Manuscript is “the version of the article accepted for publication including all changes made as a result of the peer review process, and which may also include the addition to the article by IOP Publishing of a header, an article ID, a cover sheet and/or an ‘Accepted Manuscript’ watermark, but excluding any other editing, typesetting or other changes made by IOP Publishing and/or its licensors”

This Accepted Manuscript is © 2020 IOP Publishing Ltd.

During the embargo period (the 12 month period from the publication of the Version of Record of this article), the Accepted Manuscript is fully protected by copyright and cannot be reused or reposted elsewhere.

As the Version of Record of this article is going to be / has been published on a subscription basis, this Accepted Manuscript is available for reuse under a CC BY-NC-ND 3.0 licence after the 12 month embargo period.

After the embargo period, everyone is permitted to use copy and redistribute this article for non-commercial purposes only, provided that they adhere to all the terms of the licence <https://creativecommons.org/licenses/by-nc-nd/3.0>

Although reasonable endeavours have been taken to obtain all necessary permissions from third parties to include their copyrighted content within this article, their full citation and copyright line may not be present in this Accepted Manuscript version. Before using any content from this article, please refer to the Version of Record on IOPscience once published for full citation and copyright details, as permissions will likely be required. All third party content is fully copyright protected, unless specifically stated otherwise in the figure caption in the Version of Record.

View the [article online](#) for updates and enhancements.

High-density electrophysiological recordings in macaque using a chronically implanted 128-channel passive silicon probe

Liane Klein^{1,2,3,*}, Frederick Pothof^{4,*}, Bogdan C Raducanu^{5,6}, Johanna Klön-Lipok²,
Katharine A Shapcott^{1,7}, Silke Musa⁵, Alexandru Andrei⁵, Arno AA Aarts⁸, Oliver Paul^{4,9},
Wolf Singer^{1,2,7,+}, Patrick Ruther^{4,9,+,#}

¹ Ernst Strüngmann Institute (ESI) gGmbH for Neuroscience in Cooperation with Max Planck Society, Deutschordenstraße 46, D-60528 Frankfurt am Main, Germany

² Max Planck Institute for Brain Research, Max-von-Laue-Str. 4, D-60438 Frankfurt am Main, Germany

³ Institute of Cell Biology and Neuroscience, Goethe-University Frankfurt, Max von Laue Str. 13, D-60438 Frankfurt am Main, Germany

⁴ Microsystem Materials Laboratory, Department of Microsystems Engineering (IMTEK), University of Freiburg, Georges-Koehler-Allee 103, D-79110 Freiburg, Germany

⁵ Interuniversity Microelectronics Center (imec), Kapeldreef 75, B-3001 Heverlee, Belgium

⁶ Electrical Engineering Department (ESAT), KU Leuven, Kasteelpark Arenberg 10, B-3001 Leuven, Belgium

⁷ Frankfurt Institute for Advanced Studies (FIAS), Ruth-Moufang-Str. 1, D-60438 Frankfurt am Main

⁸ ATLAS Neuroengineering bvba, B-3000 Leuven, Belgium

⁹ BrainLinks-BrainTools Cluster of Excellence at the University of Freiburg, Georges-Koehler-Allee 80, D-79110 Freiburg, Germany

*These authors have contributed equally to this work

+These authors have contributed equally to the design of this study

#Corresponding author: ruther@imtek.de

Conflict of interest Arno Aarts is co-founder and CEO of ATLAS Neuroengineering; Patrick Ruther and Oliver Paul are co-founders of ATLAS Neuroengineering; ATLAS develops silicon-based neural probes which have however not been used in this study.

Acknowledgement The present study has received funding from the European Union's Seventh Framework Program (FP7/2007-2013) under grant agreement n°600925 (NeuroSeeker), the International Max Planck Research School for Neural Circuits, Max-von-Laue-Str. 4, D-60438 Frankfurt am Main, Germany and the Ernst Strüngmann Institute for Neuroscience in cooperation with Max Planck Society.

Abstract

Objective – The analysis of interactions among local populations of neurons in the cerebral cortex (e.g. within cortical microcolumns) requires high resolution and high channel count recordings from chronically implanted laminar microelectrode arrays. The request for high-density recordings of a large number of recording sites can presently only be accomplished by probes realized using complementary metal-oxide-semiconductor (CMOS) technology. In preparation for their use in non-human primates, we aimed for neural probe validation in a head-fixed approach analyzing the long-term recording capability. *Approach* – We examined chronically implanted silicon-based laminar probes, realized using a CMOS technology in combination with micromachining, to record from the primary visual cortex (V1) of a monkey. We used a passive CMOS probe that had 128 electrodes arranged at a pitch of 22.5 μm in four columns and 32 rows on a slender shank. In order to validate the performance of a dedicated microdrive, the overall dimensions of probe and interface boards were chosen to be compatible with the final active CMOS probe with integrated circuitry. *Main results* – Using the passive probe, we recorded simultaneously local field potentials (LFP) and spiking multiunit activity (MUA) in V1 of an awake behaving macaque monkey. We found that an insertion through the dura and subsequent readjustments of the chronically implanted neural probe was possible and allowed us to record stable LFPs for more than five months. The quality of MUA degraded within the first month but remained sufficiently high to permit mapping of receptive fields during the full recording period. *Significance* – We conclude that the passive silicon probe enables semi-chronic recordings of high quality of LFP and MUA for a time span exceeding five months. The new microdrive compatible with a commercial recording chamber successfully demonstrated the readjustment of the probe position while the implemented plug structure effectively reduced brain tissue movement relative to the probe.

Keywords

high-density recording, CMOS-based laminar probe, recording chamber, chronic recording, receptive fields, visual cortex, head-fixed probe

1 Introduction

Microelectrodes have been and still are essential tools to record neuronal activity with high temporal resolution. Recently the implementation of silicon-based fabrication technologies for microelectrodes has led to breakthroughs in the attempts to obtain simultaneous recordings from large numbers of neurons. Initially, recordings were performed with single wire electrodes or tetrodes that only captured the activity of a few neurons (Hong & Lieber, 2019). For the assessment of spatially distributed assemblies of neurons in the cerebral cortex, silicon based arrays of up to 100 microelectrodes were developed (Bhandari et al., 2010). These electrode arrays have to be implanted chronically and once inserted do not allow for further adjustments of electrode positions. In order to allow simultaneous recordings of large numbers of neurons along linear tracks, silicon-based laminar probes with multiple,

1
2
3 narrowly spaced recording sites have been introduced (Wise et al., 2008). These electrodes can be
4 handled like single wire electrodes and remain adjustable in view of implantation depth following their
5 insertion. They are now widely used and commercially available in numerous different versions from
6 single shank over comb-like towards 3D neural probe arrays (Barz et al., 2017).
7
8

9
10 While the silicon probes hold large numbers of densely packed recording sites, the bottleneck is the
11 management of the wire connections between the electrodes and the amplifiers. For this reason, the
12 complementary metal-oxide-semiconductor (CMOS) technology was exploited to enable the selection
13 of subsets of electrodes (Fiáth et al., 2016; Herbawi et al., 2018; Lopez et al., 2017; Seidl et al., 2011)
14 or the sequential multiplexing of recording sites (Wise et al., 2008). High-density laminar probes
15 enabling the simultaneous recording of neural activity along the entire probe have recently become
16 available and were successfully tested in acute experiments (Raducanu et al., 2017).
17
18
19
20

21
22 Neural probes are applied in either acute or chronic experimental settings. In the case of acute
23 experiments, stereotaxic frames are typically used to insert the probes to the targeted depth and retract
24 them after data recording. In contrast, chronic experiments request a probe fixation relative to the skull
25 providing the possibility to adjust the probe position using microdrives (Dotson et al., 2017; Jovalekic
26 et al., 2017; Márton et al., 2016; Michon et al., 2016; Voigts et al., 2019; Yang et al., 2011) where a
27 probe shuttle is either operated manually (Márton et al., 2016; Michon et al., 2016; Voigts et al., 2019)
28 or motorized (Jovalekic et al., 2017; Yang et al., 2011). Depending on the applied probe type, the
29 probe shuttles comprise through-holes or hook-like structures for the fixation of wire electrodes or
30 tetrodes (Voigts et al., 2019), or are large enough to attach probes or probe interface boards using
31 adhesive bonding (Michon et al., 2016) or screws (Jovalekic et al., 2017; Márton et al., 2016). The
32 position of the shuttle is stabilized with respect to the implantation direction by friction between
33 shuttle and guiding structures (Michon et al., 2016; Voigts et al., 2019) or by using a spring (Jovalekic
34 et al., 2017; Márton et al., 2016).
35
36
37
38
39
40
41
42

43
44 The goal of the present study was to predict whether the active, high-density probes can also be
45 implanted chronically in a way that permits long-term recordings in awake animals and a continuous
46 readjustment of the probe position after insertion. To this end, we designed an insertion strategy for
47 the chronic implantation of these electrodes in the visual cortex of a macaque monkey. We tested this
48 strategy with a high density (128 contacts) passive silicon probe (Fiáth et al., 2018), whose mechanical
49 properties and electrode configuration were identical to the active probes (Raducanu et al., 2017). The
50 head-fixed microdrive allowed to insert the probes through the intact dura with their depth remaining
51 adjustable. The *in vivo* experiments yielded local field potentials (LFPs) and multiunit activity (MUA)
52 from many recording sites for more than 23 weeks.
53
54
55
56
57
58
59
60

2 Materials and methods

2.1 System overview

The recording system schematically shown in Figure 1(A) allows for chronic implantation of the 128-channel laminar silicon-based neural probe into the brain of non-human primates. The system enables to precisely set the insertion depth of the neural probe and freely adjust it once the probe has been inserted. The system design is laid-out to be compatible with a recording chamber from Gray Matter Research (Bozeman, MT, USA) using the respective implantation procedure described by the manufacturer. Key advantage of using this chamber concept is given by the established sealing approach of the brain surface against the environment preventing serious infections. Instead of using a microdrive for 32 wire electrodes, a custom designed microdrive has been implemented that is capable of handling a printed circuit board (PCB) carrying the silicon-based neural probe of larger channel count (Fiáth et al., 2018). This microdrive is fixed to the chronically implanted recording chamber using a mounting ring, as described in (Pothof et al., 2017).

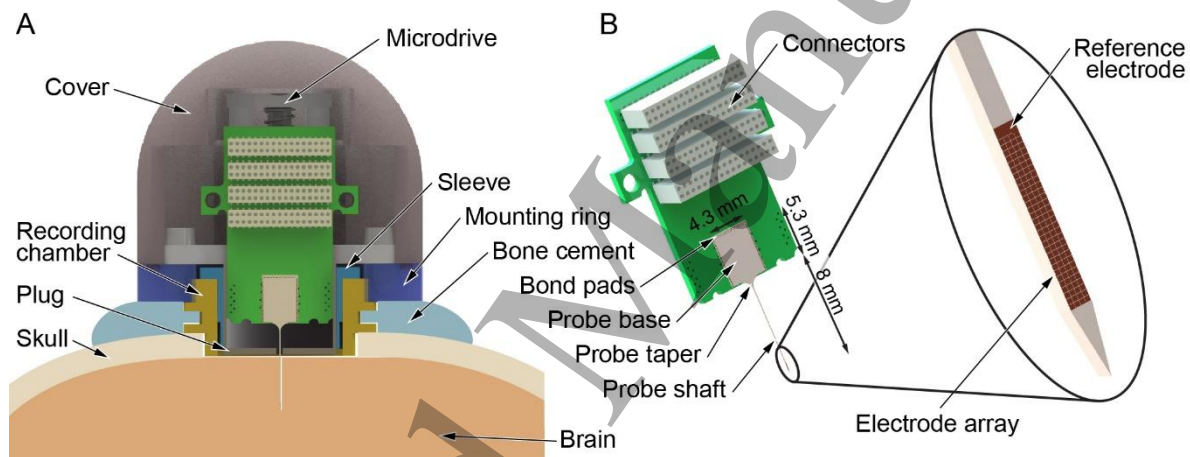


Figure 1: (A) Schematic cross-section of the entire system attached to the skull using bone cement. (B) Schematic representation of the PCB with connectors and the 128-channel silicon probe comprising TiN electrodes with lateral dimensions of $20 \mu\text{m} \times 20 \mu\text{m}$.

2.2 Silicon probe

The passive silicon probe applied in this study and its acute in vivo use in rat brains has been described earlier (Fiáth et al., 2018). In short, a $0.13 \mu\text{m}$ CMOS process is used to pattern three metal layers at a minimal linewidth of 130 nm and sandwich them in-between silicon oxide and silicon nitride insulation and passivation layers. The metal lines establish the electrical connection between the electrodes arranged as a 4×32 array at the distal section of a slender probe shank (length 8 mm , width $100 \mu\text{m}$, thickness $50 \mu\text{m}$) and bond pads distributed along the edges of the rectangular probe base ($4.3 \text{ mm} \times 5.3 \text{ mm}$), as illustrated in Figure 1(B). The quadratic recording electrodes with a side-length of $20 \mu\text{m}$ have an inter-electrode pitch of $22.5 \mu\text{m}$ such that the electrode array covers a length of ca. $700 \mu\text{m}$ along the probe shank. One electrode positioned proximally to the array has an electrode area increased by a factor of ca. 10 and can serve as a local reference electrode. The electrodes are covered

by a 600-nm-thin layer of titanium nitride (TiN) providing a reduced electrode impedance of 49.28 ± 3.29 k Ω at 1 kHz (Fiáth et al., 2018). The probe shape and shank thickness are defined by a process similar to the etching before grinding approach described elsewhere (Herwik et al., 2011). A photograph of the entire probe is shown in Figure 2(A) together with an enlarged optical micrograph of the electrode array in Figure 2(B).

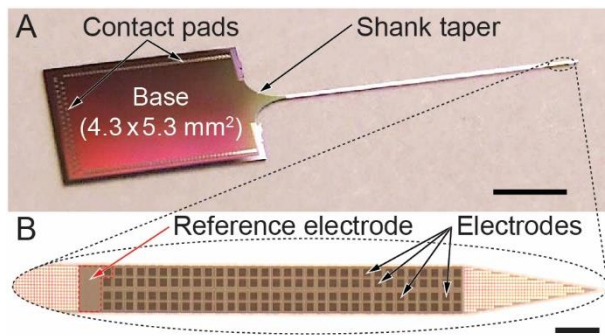


Figure 2: (A) Optical photograph of the 128-channel silicon probe and (B) detail of the tip region with the high-density TiN electrode array (Scale bars: (A) 2 mm, (B) 100 μ m).

The 128-channel silicon probe is assembled on a PCB (length 20.75 mm, Figure 1(B)) and wire bonded to respective contact pads. The compact PCB fits into the Gray Matter Research recording chamber and carries four 32-ch Omnetics connectors (NPD-36-VV-GS, Omnetics Connector Corporation, Minneapolis, MN, USA). During recording, the connectors are interfaced to four headstages from Tucker-Davis Technologies (Alachua, FL, USA) using 10-cm-long compact flexible ribbon cables with the recording chamber used as ground connection. The PCB is fixed on the shuttle of the microdrive using two set screws (Figure 3).

2.3 Recording chamber

We used the Gray Matter Research tangential recording chamber (outer diameter \sim 20 mm) combined with a custom-made titanium mounting ring (inner diameter 18 mm, outer diameter 30 mm), as previously described (Pothof et al., 2017), that is screwed onto the upper section of the chamber. The recording chamber and thus the brain surface are sealed against the environment by a silastic membrane held in place using a sleeve screwed into the cylindrical chamber (Figure 1(A)). The silicon probe with pointy tip (Barz et al., 2017) is capable of penetrating the silastic membrane (Gray et al., 2007) without harming its sealing functionality.

2.4 Microdrive

The cross-sectional view of the custom-designed microdrive used to position the silicon probe inside the brain and precisely adjust the implantation depth is shown in Figure 3(A). The drive comprises a shuttle which holds the silicon probe assembled on its PCB. The shuttle is guided by two guide posts vertically assembled between a base plate and a top plate. The vertical shuttle position is adjusted using a M2.5 screw, resulting in a precision of 450 μ m/turn. Further, the backlash of the shuttle position due to thread tolerances is minimized using a spring mounted between the top plate and the

1
2
3 shuttle. The drive can be fixed on the mounting ring in 16 different orientations with respect to the
4 recording chamber. As the probe on the shuttle is mounted off-center by approximately 0.3 mm, this
5 corresponds to 16 probe positions within the recording chamber located on a circle with a diameter of
6 ca. 0.5 mm. Once the desired implantation depth is reached, two set screws fix the position of the
7 shuttle to the guide posts. For changing the depth to address different cortical layers, the set screws
8 have to be untightened first, then the new probe implantation depth can be set.
9
10

11
12
13 Due to the mechanical flexibility of the silastic membrane sealing the brain surface, a vertical
14 movement of the brain tissue, e.g. due to blood pulsation or an acceleration of the skull, cannot be
15 prohibited. This will cause a relative movement between the chamber-fixed neural probe and the
16 surrounding tissue, affecting the signal quality and ultimately influencing the long-term recording
17 capability (Chauvière et al., 2019; Pothof et al., 2017). In order to minimize this brain movement, a
18 cylindrical plug, as shown in Figures 1(A) and 3(A), is used in our approach. Its height is designed
19 such that it is in direct contact with the silastic membrane thus minimizing the brain movement. It has
20 a hole of 1.5 mm in diameter which is 0.3 mm off center with respect to the cylindrical recording
21 chamber. The silicon probe can be advanced through the center of this hole to penetrate the silastic
22 membrane and the dura mater into the cortex.
23
24
25
26
27
28

29
30 All components used for the microdrive are made of titanium, except for the stainless steel spring. In
31 order to improve gliding of the shuttle over the guide pins, all surfaces were spray coated with a thin
32 layer of medical grade PTFE. The base plate of the microdrive is adhesively fixed to the plug using the
33 adhesive EPO-TEK 301-2 (Epoxy Technology, Inc., Billerica, MA, USA). The guide posts are solely
34 press-fitted into holes in the base and top plates. Figure 3(B) shows the Gray Matter Research
35 recording chamber combined with the mounting ring, the microdrive and the PCB carrying the 128-
36 channel neural probe from different perspectives.
37
38
39
40
41
42
43
44
45
46
47
48
49
50
51
52
53
54
55
56
57
58
59
60

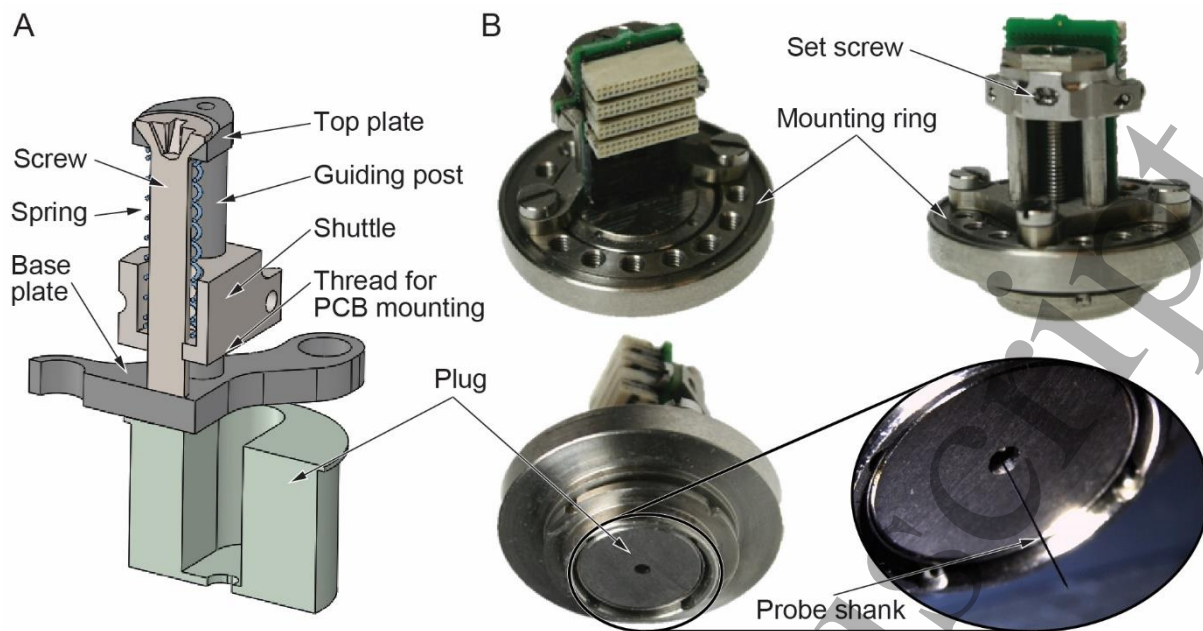


Figure 3: Implanted microdrive mounted on top of the recording chamber from Gray Matter Research. (A) Schematic cross-section of the microdrive. (B) Photographs from different perspectives of the microdrive with PCB carrying the 128-channel silicon probe. The microdrive is fixed to the mounting ring using three screws (B-top), the plug (B-bottom) used to minimize the brain movement is adhesively attached to the microdrive base plate.

2.5 Surgery

This study was conducted on one female *macaca fascicularis* (16 years old, 5.5 kg). All experimental procedures were approved by the local authorities (License number F149/1001; Regierungspräsidium, Hessen, Darmstadt) and are in accordance with the “European Union’s Directive 2010/63/EU”.

All surgical procedures were carried out under aseptic conditions. Anesthesia was induced by i. m. injections of 0.01 mg/kg Robinul followed by a mixture of Ketamine (5 mg/kg) and Medetomidine (0.02 mg/kg) and sustained by controlled ventilation combined with Isoflurane (in O₂) and intravenous administration of Remifentanyl (0.08-0.09 µg /kg/min). Postsurgical analgesic and antibiotic care was administered according to the authorized guidelines during the following days.

For a preceding study, a custom fitted titanium head-holder base plate had been fixed with titanium bone screws to the skull. This base plate was complemented with a bolt to stabilize the head position, allowing stable eye control during the experiments.

For implantation of the recording chamber (see Section 2.3), a circular craniotomy was performed over the left primary visual cortex (V1). The craniotomy position was planned to cover a para- to perifoveal V1 area, by using magnetic resonance imaging (MRI) and computer tomography (CT) scan results and a stereotactic brain atlas (Paxinos et al., 2008).

After a preceding study (Chauvière et al., 2019) was finished, the microdrive and probe of that study were removed, and the sleeve with silastic membrane was exchanged. A plug (Gray et al., 2007) was inserted into the chamber, which was sealed with a flat titanium cap. The chamber was frequently

checked for infections, which did not occur. More than a year elapsed before our study started. As bone had grown in that time underneath the recording chamber, the craniotomy had to be renewed and a fresh sleeve with silastic membrane was inserted. The bone growth caused an additional gap between the recording chamber and dura.

2.6 Probe insertion

The probe was inserted in the awake behaving monkey 17 days after the renewed craniotomy. Due to the construction of the microdrive (Figure 3(B)), the actual penetration of the dura could not be visually observed. Instead the penetration into the cortex was monitored by continuous electrophysiological recordings. Dural dimpling, which we could not observe, is reported to be reduced by the silastic membrane (Gray et al., 2007).

2.7 In vivo electrophysiological recordings

Each electrode's signal was amplified and digitized at a rate of 25 kHz. They were band-pass filtered between 0.1 and 300 Hz to obtain LFPs and between 300-4000 Hz to gather MUA (Tucker-Davis Technologies). For referencing and grounding of the probe we used the recording chamber and did not use the reference electrode for additional local re-referencing. The MUA was quantified by adjusting a threshold for spikes that was set at 3.5 standard deviation above the noise level determined at the beginning of each recording session.

The monkey had been trained to fixate a central spot on a monitor (Samsung Screen Master 2233, 120 Hz refresh rate) of 47 cm × 29.4 cm (width × height) placed 64 cm in front of the eye plane and to signal a change of the fixation spot by manipulating a lever. Eye fixation was controlled using an infrared sensitive camera (Thomas RECORDING GmbH) and custom-written MATLAB scripts using PsychToolbox (Brainard, 1997). For correctly completed trials (no fixation breaks and punctual lever responses) the monkey received water or water-diluted juice as reward.

We evoked neuronal responses by presenting visual stimuli on the monitor. In order to map the receptive fields (RF) of the neurons recorded from the different electrode sites, a passive viewing task was conducted. While the monkey fixated a green fixation spot in the screen center, a single white bar crossed the screen in one of 16 possible directions. The orientation of the bar was orthogonal to its sweeping direction. After the stimulus crossed the screen and an additional jittered delay the fixation spot changed its color from green to pink cuing the monkey's lever-response. If the monkey responded within a 2500 ms time window and without fixation break, a liquid reward was given.

Following the same behavioral protocol, whole field flash stimuli (duration: 200 ms) were presented to elicit stimulus locked MUA responses and evoked potentials (LFPs). Response averages were calculated from at least 60 stimulus presentations per recording session. All behavioral tasks were conducted using a custom-written visual stimulation presentation package in MATLAB, relying on the PsychToolbox library (Brainard, 1997).

2.8 Analyses

All analyses were performed with custom-written programs in MATLAB 2014a using the FieldTrip toolbox (Oostenveld et al., 2011). The RF locations were computed using the neuronal responses to the receptive field bar mapping paradigm described in Section 2.7. For full details of the analysis procedure refer to (Fiorani et al., 2014). In short, we used the back-projection algorithm to compute a z-scored 2D RF map at the optimal delay for each contact. A threshold of 1.6 z-score was chosen as a cut-off for the inclusion of the contact point in the further analyses. Only if the maximal activity surpassed this threshold, it was judged to have a sufficient signal-to-noise ratio (SNR) to be considered a RF. A 2D Gaussian was then fitted to the RF maps which passed the inclusion threshold. The center of the 2D Gaussian fitted to the RF map was used to estimate the RF center location.

We calculated the percentage change of flash-induced MUA responses (Figure 6(A)) by first calculating the trial averaged peristimulus time histogram (PSTH). We then identified both the flash-induced maximum and the average baseline (200 ms interval before flash onset) firing rate. Next, the difference between the maximum and average baseline firing rate was divided by the baseline average and the result multiplied by 100 to express changes in response amplitude in percent.

3 Results

After the initial insertion of the passive laminar probe, we found that 126 out of the 128 contacts recorded neuronal signals. The remaining two contacts were not working (see Figure 4(A)) and did not recover over the next 5 months of recording. The moving bar stimuli used to determine the position of the RFs (Section 2.7) elicited vigorous MUA responses on 126 of 128 contacts, including the larger contact that mimicked a reference. This reference contact was implemented on the passive probe for test purposes in preparation for the design of the CMOS-based active probe with multiple reference electrodes along the entire probe shank (Raducanu et al., 2017). As expected from the laminar arrangement of the recording sites, the RF positions were overlapping and concentrated within an area of $0.4^\circ \times 0.5^\circ$ visual angle (height \times width) (see Figure 4(B, C) and Section 2.8). This confirms that the trajectory of the probe was approximately perpendicular to the cortical surface. Flash-evoked LFPs (Figure 4(A)) were very similar for adjacent recording sites but changed gradually with recording depth, as expected. The overall latency decreased with increasing depth and the amplitude and polarity of the various components changed gradually (see Figure 4(A)). These conditions remained stable and reproducible over the whole recording period, i.e. 23 weeks. The comparison of Figures 5(A) and (C) shows that stimulus-induced LFP responses were very similar 6 days and 5 months post-insertion.

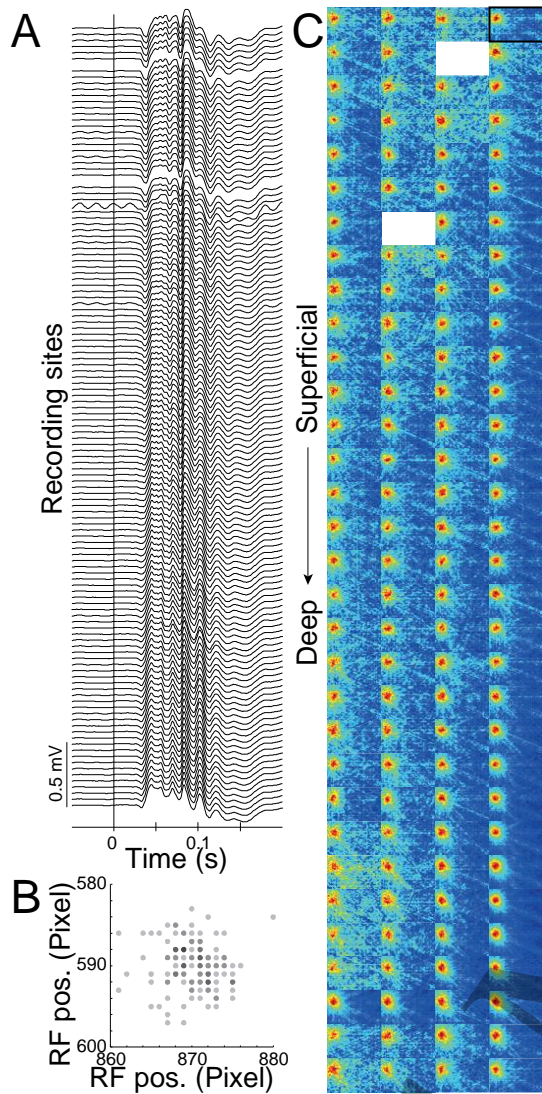


Figure 4: Early example recording after electrode insertion. (A) Laminar profile of averaged ($N = 149$ trials) flash evoked LFP responses. Traces are ordered according to the arrangement of contact points (compare to C) from left to right and top to bottom. (B) Location of the RF centers of neurons recorded from 126 sites. Darker points indicate multiple overlapping RF centers. (C) RF of neurons sampled at the 126 functioning contacts of the probe. The orientation of the RF maps corresponds to the contact order (see Figure 2(B)). The bottom row faces the probe's tip. The reference contact recorded sufficient MUA signal to calculate a RF map (upper right corner, highlighted by the black frame).

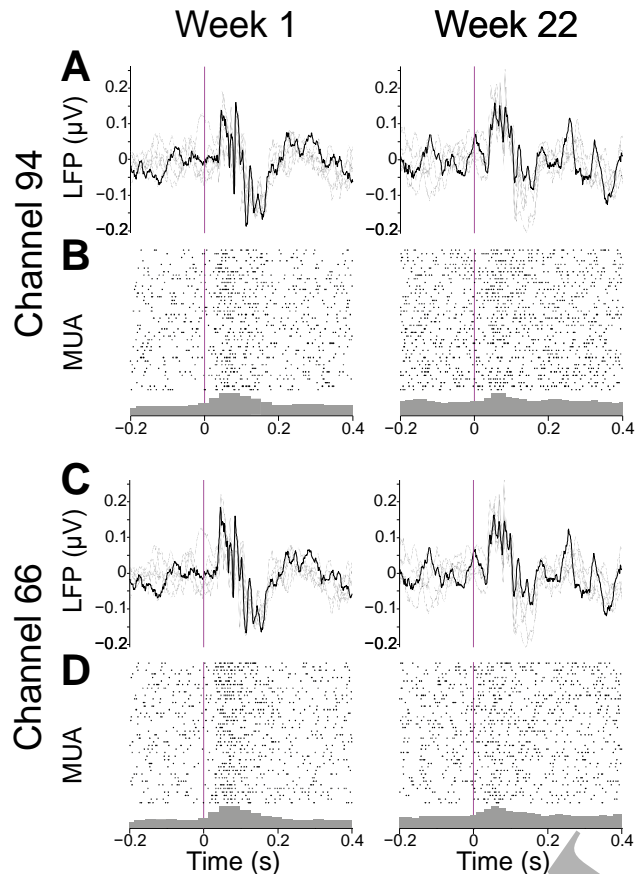


Figure 5: Examples of signal quality over time. (A-B & C-D Example recordings of flash evoked neuronal responses in primate V1 for two exemplary channels). The left column was recorded 6 days, and the right column 5 months after probe insertion. The magenta line at time 0 shows the flash onset. (A, C) Example LFP trace of one randomly selected correct trial (black) and 5 additional random correct trials (gray). Time axes as in B, D. Note that the LFP of each channel is similar between both sessions. (B, D) Example MUA raster plots from 6 correct trials as in A&C and 34 additional randomly selected correct trials (one trial per row). Normalized histograms for the respective responses are shown below (peak equals 1). Note that in the later session flash-evoked MUA is still recordable.

After ensuring that we had stable recording conditions, we next took advantage of the fact that the microdrive enabled us to readjust the probe's depth position. As the high-density recording sites spanned only 700 μm of the shank length, we could not record simultaneously from all cortical layers. Therefore, we moved the probe in order to sample from several cortical layers. We varied the probe depth at the end of recording sessions in order to allow stabilization of recording conditions before the next recording day. The maximally achieved cortex coverage (distance between lowest and highest possible recording position) was ~ 1.6 mm. Due to bone growth (Section 2.5) which caused an additional gap between recording chamber and dura, this cortical travel distance was not the theoretical maximum. The maximum travel distance was reached 13 weeks post-insertion.

After a recording break, we restarted recordings and systematically retracted the probe after every recording day by ~ 113 μm and mapped the RFs of neurons recorded from the different recording sites. As shown in Figure 6(B), we were still able to characterize RFs. Thus, the recording sites were still

able to capture neuronal discharges several months after implantation. Moreover, the RF properties of the neurons seemed normal, indicating that the numerous adjustments of probe position had not caused any major damage to the cortical tissue surrounding the probe. However, the comparison of Figures 5(B, D) and 6(A) shows that the SNR of MUA recordings decreased after the first week of recording. For some recording sites, the initial SNR could be recovered by small movements of the probe, suggesting that deterioration of the contact points was not the primary reason for this decrease in recording quality. Additionally, we were able to detect a few examples of putative single unit activity (SUA) by hand tuning time-amplitude window discriminators (Santhanam et al., 2004) both a few weeks and several months after implantation, although at a reduced SNR with time (data not shown), as with the LFP and MUA data.

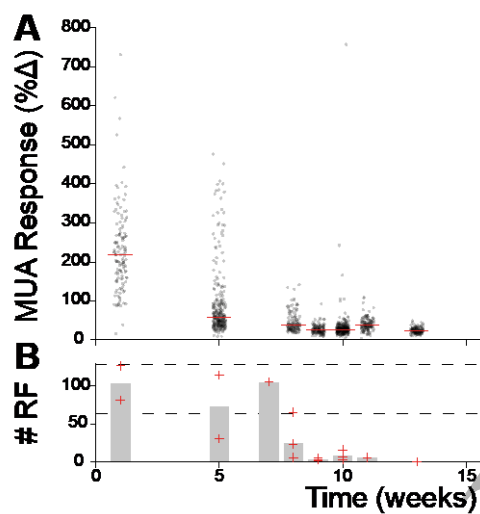


Figure 6: Visually evoked MUA responses over time. (A) Amplitude of flash evoked MUA responses relative to baseline in %. Averaged signals from active contact points (black dots) for all flash-evoked recordings were pooled per calendar week (red lines show weeks' medians, from left to right $N = 128, 256, 127, 128, 254, 127, 128, 256, 127, 383, 256$). Note that MUA responses decrease drastically after the first week, but flash-evoked spiking can still be observed at week 23. (B) Mean number of all detected RFs per calendar week. Gray bars show the weeks' mean RFs, red pluses depict the single sessions. The dotted lines indicate 128 and 64 RFs, respectively, which amounts to 100% and 50% of the possible RFs per session. The gaps are caused by conducting other recording paradigms or pauses in recording.

4 Discussion

In this study we introduce an implantation technique for long-term chronic recording from a position-adjustable high-density laminar probe and show that stable recordings can be obtained for more than 23 weeks. The probe maintained its integrity after penetrating both a silastic membrane of the recording chamber and the dura. Furthermore, the probe continued to record neural activity reliably despite numerous depth adjustments.

The novel microdrive was designed such that it fits to a commercially available recording chamber and at the same time will enable hosting highly advanced, CMOS-based neural probes, as developed and

1
2
3 introduced by the NeuroSeeker consortium of the EU-funded research project (Raducanu et al., 2017).
4 Our system successfully demonstrated that silicon-based probe fixed relative to the skull can easily be
5 inserted and retracted using the same device. This provides a clear indication that even larger probe
6 systems using a hybrid integration of CMOS probe and headstage can be hosted on the microdrive.
7 The slightly asymmetric layout provided multiple insertion positions within the recording chamber.
8 This allows us to circumvent the penetration of previously penetrated brain positions with potentially
9 scared tissue and blood vessels which might not have been visible in the MR scans used for surgery
10 planning.

11
12
13
14
15
16 As expected, LFP recordings remained stable over the whole test period but there was a deterioration
17 of the SNR for the MUA (see Figure 6). During the first recording week we were able to map on
18 average more than 100 RFs, but after week 7 the average number of mappable RFs dropped below 64
19 (less than 50% of contact points). This decrease in signal strength is likely due to changes of the
20 contact points and tissue reactions in the microenvironment of the contacts. Mechanical failures of the
21 probe could be excluded as the SNR for a given contact site could change in either direction over
22 subsequent recording sessions or after the adjustments of the probe position (Campbell & Wu, 2018).
23 The most likely cause are thus biological responses to the probe, as indicated by numerous studies
24 showing that probe insertion causes damage of the blood-brain-barrier, which in turn results in an
25 immune response against foreign bodies (Campbell & Wu, 2018; Kozai et al., 2015; Salatino et al.,
26 2017). One outcome can be neuronal cell death, which could account for the reduction in mappable
27 RFs. Another result of the foreign body response is glial encapsulation which has previously been
28 shown to be one of the major factors for impedance increases of electrodes (Campbell & Wu, 2018;
29 Kozai et al., 2015; Salatino et al., 2017). An impedance increase, in turn, decreases the SNR.
30 However, slow advancement of the probe into fresh tissue ((Kozai et al., 2015); until week 13) did not
31 substantially improve the overall MUA quality, suggesting rather global tissue reactions or changes of
32 the contacts to be major reasons for the decrease in MUA quality. Nonetheless, after a recording break
33 preceding week 20, we observed improvements in MUA quality. This improvement could be caused
34 by an impedance decrease, which previously has been shown to occur after 12 weeks post-insertion
35 (Campbell & Wu, 2018). The process behind this recovery is not yet fully understood. Literature
36 suggests that it is caused by the glial encapsulation starting to grow denser and thinner at the same
37 time (Campbell & Wu, 2018). As we did not observe complete recovery of recording quality following
38 changes in electrode position, it is likely that both physico-chemical changes at the contact sites, as
39 well as tissue reactions were responsible for the decrease in SNR. A previous study using the same
40 probe design showed that large numbers of single units could be isolated in mouse, rat and cat models
41 (Fiáth et al., 2018). In our study we made no systematic attempts to determine the fraction of sortable
42 spikes. However, we could observe that the action potentials of individual cells were picked up by
43 adjacent contacts (data not shown). This would allow the application of automatic and semi-automatic
44 sorting algorithms developed for tetrode or high-density recordings.

Based on the successful long-term recordings applying mechanically stiff neural probes in a skull-fixed approach, as demonstrated in this study and a recent publication by Chauvière et al. (Chauvière et al., 2019), we plan to extend this experimental protocol to the most advanced CMOS-based neural probes currently available (Dimitriadis et al., 2018; Raducanu et al., 2017). In this case, the PCB hosting the CMOS-probe is equipped with additional electronic components and a single connector for the external instrumentation (Raducanu et al., 2017). This renders the probe PCB more compact in comparison to the one used in this study. Further, as the shank of the advanced CMOS probe is completely covered by electrodes (Raducanu et al., 2017), two application scenarios are foreseen. Similar to this study, the probe might be translated longitudinally using a microdrive to improve signal quality, as demonstrated here. The second scenario would mold the probe-carrying PCB into a polymeric plug. Once the plug is introduced into the recording chamber, the probe position is fixed relative to the tissue during the entire duration of the experiment while brain movements are minimized. Nonetheless, the complete coverage of the probe shank with recording sites would provide simultaneous access to all cortical layers penetrated by the neural probe. As an alternative, neural probes with compact probe bases, as demonstrated by Herbawi et al. (Herbawi et al., 2018) and De Dorigo et al. (De Dorigo et al., 2018), interfaced to highly flexible ribbon cables would allow to reduce the shuttle size and thus the overall dimensions of the microdrive. In consequence, it is foreseeable to implement multiple CMOS probes using an equivalent number of drives providing access to larger brain volumes.

5 Conclusion

We have shown that chronic recordings with high-density silicon probes are feasible. It is our belief that the CMOS technology will play an essential role in furthering our understanding of information processing in complex and distributed neuronal networks and to complement optical recording techniques. The latter, especially if calcium-dependent, still suffer from limitations, even though they excel in their ability to track responses from optically identified neurons over long time periods. The major limitations of temporal resolution and obtaining massive parallel recording from deep or widely distributed areas are overcome when recording with microelectrodes, such as high-density CMOS probes.

6 References

Barz, F., Livi, A., Lanzilotto, M., Maranesi, M., Bonini, L., Paul, O., & Ruther, P. (2017). Versatile, modular three-dimensional microelectrode arrays for neuronal ensemble recordings: From design to fabrication, assembly, and functional validation in non-human primates. *Journal of Neural Engineering*, *14*, 036010-036010 (16pp). <https://doi.org/10.1088/1741-2552/aa5a90>

- 1
2
3 Bhandari, R., Negi, S., & Solzbacher, F. (2010). Wafer-scale fabrication of penetrating neural
4
5 microelectrode arrays. *Biomed Microdevices*, *12*(5), 797–807. <https://doi.org/10.1007/s10544->
6
7 010-9434-1
8
- 9 Brainard, D. H. (1997). The Psychophysics Toolbox. *Spatial Vision*, *10*(4), 433–436.
10
- 11 Campbell, A., & Wu, C. (2018). Chronically Implanted Intracranial Electrodes: Tissue Reaction and
12
13 Electrical Changes. *Micromachines*, *9*(9), 430. <https://doi.org/10.3390/mi9090430>
14
- 15 Chauvière, L., Pothof, F., Gansel, K. S., Klon-Lipok, J., Aarts, A. A. A., Holzhammer, T., Paul, O.,
16
17 Singer, W. J., & Ruther, P. (2019). In vivo Recording Quality of Mechanically Decoupled
18
19 Floating Versus Skull-Fixed Silicon-Based Neural Probes. *Frontiers in Neuroscience*, *13*, 464.
20
21 <https://doi.org/10.3389/fnins.2019.00464>
22
- 23 De Dorigo, D., Moranz, C., Graf, H., Marx, M., Wendler, D., Shui, B., Sayed Herbawi, A., Kuhl, M.,
24
25 Ruther, P., Paul, O., & Manoli, Y. (2018). Fully Immersible Subcortical Neural Probes With
26
27 Modular Architecture and a Delta-Sigma ADC Integrated Under Each Electrode for Parallel
28
29 Readout of 144 Recording Sites. *IEEE Journal of Solid-State Circuits*, *53*(11), 3111–3125.
30
31 <https://doi.org/10.1109/JSSC.2018.2873180>
32
- 33 Dimitriadis, G., Neto, J. P., Aarts, A., Alexandru, A., Ballini, M., Battaglia, F., Calcaterra, L., David,
34
35 F., Fiath, R., Frazao, J., Geerts, J., Gentet, L. J., Helleputte, N. V., Holzhammer, T., Hoof, C.
36
37 van, Horvath, D., Lopes, G., Maris, E., Marques-Smith, A., ... Kampff, A. R. (2018). Why not
38
39 record from every channel with a CMOS scanning probe? *BioRxiv*.
40
41 <https://doi.org/10.1101/275818>
42
- 43 Dotson, N. M., Hoffman, S. J., Goodell, B., & Gray, C. M. (2017). A Large-Scale Semi-Chronic
44
45 Microdrive Recording System for Non-Human Primates. *Neuron*, *96*(4), 769-782.e2.
46
47 <https://doi.org/10.1016/j.neuron.2017.09.050>
48
- 49 Fiáth, R., Beregszászi, P., Horváth, D., Wittner, L., Aarts, A. A. A., Ruther, P., Neves, H. P., Bokor,
50
51 H., Acsady, L., & Ulbert, I. (2016). Large-scale recording of thalamocortical circuits: In vivo
52
53 electrophysiology with the two-dimensional electronic depth control silicon probe. *Journal of*
54
55 *Neurophysiology*, *116*(5), 2312–2330. <https://doi.org/10.1152/jn.00318.2016>
56
57
58
59
60

- 1
2
3 Fiáth, R., Raducanu, B. C., Musa, S., Andrei, A., Lopez, C. M., Hoof, C. van, Ruther, P., Aarts, A.,
4
5 Horváth, D., & Ulbert, I. (2018). A silicon-based neural probe with densely-packed low-
6
7 impedance titanium nitride microelectrodes for ultrahigh-resolution in vivo recordings.
8
9 *Biosensors and Bioelectronics*, 106, 86–92. <https://doi.org/10.1016/j.bios.2018.01.060>
10
11 Fiorani, M., Azzi, J. C. B., Soares, J. G. M., & Gattass, R. (2014). Automatic mapping of visual cortex
12
13 receptive fields: A fast and precise algorithm. *Journal of Neuroscience Methods*, 221, 112–
14
15 126. <https://doi.org/10.1016/j.jneumeth.2013.09.012>
16
17
18 Gray, C. M., Goodell, B., & Lear, A. (2007). Multichannel Micromanipulator and Chamber System
19
20 for Recording Multineuronal Activity in Alert, Non-Human Primates. *Journal of*
21
22 *Neurophysiology*, 98(1), 527–536. <https://doi.org/10.1152/jn.00259.2007>
23
24 Herbawi, A. S., Christ, O., Kiessner, L., Mottaghi, S., Hofmann, U. G., Paul, O., & Ruther, P. (2018).
25
26 CMOS Neural Probe With 1600 Close-Packed Recording Sites and 32 Analog Output
27
28 Channels. *Journal of Microelectromechanical Systems*, 27(6), 1023-1034.
29
30 <https://doi.org/10.1109/JMEMS.2018.2872619>
31
32
33 Herwik, S., Paul, O., & Ruther, P. (2011). Ultrathin Silicon Chips of Arbitrary Shape by Etching
34
35 Before Grinding. *Microelectromechanical Systems, Journal Of*, 20(4), 791–793.
36
37 <https://doi.org/10.1109/JMEMS.2011.2148159>
38
39 Hong, G., & Lieber, C. M. (2019). Novel electrode technologies for neural recordings. *Nature Reviews*
40
41 *Neuroscience*, 20(6), 330–345. <https://doi.org/10.1038/s41583-019-0140-6>
42
43 Jovalekic, A., Cavé-Lopez, S., Canopoli, A., Ondracek, J. M., Nager, A., Vyssotski, A. L., &
44
45 Hahnloser, R. H. R. (2017). A lightweight feedback-controlled microdrive for chronic neural
46
47 recordings. *Journal of Neural Engineering*, 14(2), 026006. <https://doi.org/10.1088/1741->
48
49 [2552/aa5848](https://doi.org/10.1088/1741-2552/aa5848)
50
51
52 Kozai, T. D. Y., Jaquins-Gerstl, A. S., Vazquez, A. L., Michael, A. C., & Cui, X. T. (2015). Brain
53
54 Tissue Responses to Neural Implants Impact Signal Sensitivity and Intervention Strategies.
55
56 *ACS Chemical Neuroscience*, 6(1), 48–67. <https://doi.org/10.1021/cn500256e>
57
58 Lopez, C. M., Putzeys, J., Raducanu, B. C., Ballini, M., Wang, S., Andrei, A., Rochus, V., Vandebriel,
59
60 R., Severi, S., Hoof, C. V., Musa, S., Helleputte, N. V., Yazicioglu, R. F., & Mitra, S. (2017).

1
2
3 A Neural Probe With Up to 966 Electrodes and Up to 384 Configurable Channels in 0.13 μm
4 SOI CMOS. *IEEE Transactions on Biomedical Circuits and Systems*, 11(3), 510–522.

5
6
7 <https://doi.org/10.1109/TBCAS.2016.2646901>

8
9 Márton, G., Baracska, P., Cseri, B., Plósz, B., Juhász, G., Fekete, Z., & Pongrácz, A. (2016). A
10 silicon-based microelectrode array with a microdrive for monitoring brainstem regions of
11 freely moving rats. *Journal of Neural Engineering*, 13(2), 026025.

12
13
14
15 <https://doi.org/10.1088/1741-2560/13/2/026025>

16
17 Michon, F., Aarts, A., Holzhammer, T., Ruther, P., Borghs, G., McNaughton, B., & Kloosterman, F.
18 (2016). Integration of silicon-based neural probes and micro-drive arrays for chronic recording
19 of large populations of neurons in behaving animals. *Journal of Neural Engineering*, 13(4),
20 046018–046018. <https://doi.org/10.1088/1741-2560/13/4/046018>

21
22
23
24
25 Oostenveld, R., Fries, P., Maris, E., & Schoffelen, J.-M. (2011). FieldTrip: Open Source Software for
26 Advanced Analysis of MEG, EEG, and Invasive Electrophysiological Data. *Computational*
27
28
29
30
31
32
33
34
35
36
37
38
39
40
41
42
43
44
45
46
47
48
49
50
51
52
53
54
55
56
57
58
59
60
Intelligence and Neuroscience, 2011, 1–9. <https://doi.org/10.1155/2011/156869>

Paxinos, G., Huang, X.-F., Petrides, M., & Toga, A. (2008). The Rhesus monkey brain: In stereotaxic
coordinates. In *Faculty of Health and Behavioural Sciences—Papers (Archive) (2nd ed.)*.
Retrieved from <https://ro.uow.edu.au/hbspapers/3611>.

Pothof, F., Chauvière, L., Holzhammer, T., Aarts, A. A. A., Paul, O., Singer, W., & Ruther, P. (2017).
Comparison of the in-vivo neural recording quality of floating and skull-fixed silicon probes.
158–161. <https://doi.org/10.1109/NER.2017.8008316>

Raducanu, B. C., Yazicioglu, R. F., Lopez, C. M., Ballini, M., Putzeys, J., Wang, S., Andrei, A.,
Rochus, V., Welkenhuysen, M., Helleputte, N. van, & others. (2017). Time Multiplexed
Active Neural Probe with 1356 Parallel Recording Sites. *Sensors*, 17(10), 2388–2388.
<https://doi.org/10.3390/s17102388>

Salatino, J. W., Ludwig, K. A., Kozai, T. D. Y., & Purcell, E. K. (2017). Glial responses to implanted
electrodes in the brain. *Nature Biomedical Engineering*, 1(11), 862–877.
<https://doi.org/10.1038/s41551-017-0177-7>

- 1
2
3 Santhanam, G., Sahani, M., Ryu, S. I., & Shenoy, K. V. (2004). An extensible infrastructure for fully
4 automated spike sorting during online experiments. *Conf Proc IEEE Eng Med Biol Soc.*, 2,
5 4380–4384. <https://doi.org/DOI: 10.1109/IEMBS.2004.1404219>
6
7
8
9 Seidl, K., Herwik, S., Torfs, T., Neves, H. P., Paul, O., & Ruther, P. (2011). CMOS-based high-
10 density silicon microprobe arrays for electronic depth control in intracortical neural recording.
11 *Microelectromechanical Systems, Journal Of*, 20(6), 1439–1448.
12
13 <https://doi.org/10.1109/JMEMS.2011.2167661>
14
15
16
17 Voigts, J., Newman, J. P., Wilson, M. A., & Harnett, M. T. (2019). *An easy-to-assemble, robust, and*
18 *lightweight drive implant for chronic tetrode recordings in freely moving animals* [Preprint].
19
20 Neuroscience. <https://doi.org/10.1101/746651>
21
22
23
24 Wise, K. D., Sodagar, A. M., Yao, Y., Gulari, M. N., Perlin, G. E., & Najafi, K. (2008).
25
26 Microelectrodes, Microelectronics, and Implantable Neural Microsystems. *Proceedings of the*
27 *IEEE*, 96(7), 1184–1202. <https://doi.org/10.1109/JPROC.2008.922564>
28
29
30 Yang, S., Cho, J., Lee, S., Park, K., Kim, J., Huh, Y., Yoon, E.-S., & Shin, H.-S. (2011). Feedback
31 controlled piezo-motor microdrive for accurate electrode positioning in chronic single unit
32 recording in behaving mice. *Journal of Neuroscience Methods*, 195(2), 117–127.
33
34
35
36
37 <https://doi.org/10.1016/j.jneumeth.2010.09.006>
38
39
40
41
42
43
44
45
46
47
48
49
50
51
52
53
54
55
56
57
58
59
60